

This item is the archived peer-reviewed author-version of:

The quest for value-added products from CO_2 and H_2O in a dielectric barrier discharge : a chemical kinetics study

Reference:

Snoeckx Ramses, Ozkan Alp, Reniers Francois, Bogaerts Annemie.- The quest for value-added products from CO_2 and H_2O in a dielectric barrier discharge : a chemical kinetics study
Chemoschem - ISSN 1864-5631 - 10:2(2017), p. 409-424
Full text (Publisher's DOI): <http://dx.doi.org/doi:10.1002/CSSC.201601234>
To cite this reference: <http://hdl.handle.net/10067/1398800151162165141>

The Quest For Value-Added Products From CO₂ And H₂O In A Dielectric Barrier Discharge: A Chemical Kinetics Study

Ramses Snoeckx,^{[a]*} Alp Ozkan,^[b] Francois Reniers^[b] and Annemie Bogaerts^[a]

Dedication ((optional))

Abstract: Recycling of carbon dioxide by its conversion into value-added products has gained significant interest due to the role it can play for use in an anthropogenic carbon cycle. The combined conversion with H₂O could even mimic the natural photosynthesis process. An interesting gas conversion technique currently being considered in the field of CO₂ conversion is plasma technology. To investigate whether it is also promising for this combined conversion, we performed a series of experiments and developed a chemical kinetics plasma chemistry model for a deeper understanding of the process. The main products formed are the syngas components CO and H₂, as well as O₂ and H₂O₂, while methanol formation is only observed in the ppb to ppm range. The syngas ratio, on the other hand, can easily be controlled by varying both the water content and/or energy input. Based on the model, which was validated with the experimental results, a chemical kinetics analysis is performed, which allows to construct and investigate the different pathways leading to the observed experimental results, and to clarify these results. This approach allows us to evaluate this technology based on its underlying chemistry and to propose solutions on how to further improve the formation of value-added products using plasma technology.

Introduction

Throughout history the use of natural resources has played a major role in the development of the human race. Among those resources, fossil fuels have contributed to a fast and unprecedented development in human society. However, this comes with a great cost, since burning fossil fuels leads to the emission of large amounts of the greenhouse gas CO₂. Due to the fact that these anthropogenic CO₂ emissions outpace the natural carbon cycle, the atmospheric CO₂ concentrations have been increasing from 280 ppm since the beginning of the industrial revolution to 400 ppm in 2014.^[1] With a high certainty it is this

increase that leads to the current adverse global environmental climate changes.^[1]

Utilization of this waste (CO₂) and converting it into a new feedstock (raw materials for the chemical industry and fuels) does not only comply with the framework of sustainable/green chemistry^[2,3] but also fits within the “cradle-to-cradle” concept.^[4] By generating useful products out of CO₂ we create the possibility to effectively close the carbon loop.

An interesting co-reactant to pursue this, is water. It is not only the most ubiquitous and cheapest hydrogen source, compared to CH₄ and H₂, but in addition, converting CO₂ in combination with H₂O to produce value-added products using renewable energy, would successfully mimic the natural photosynthetic process.^[5] Indeed, the successful development of artificial photosynthesis technology is no longer a fairy tale. Furthermore, water is always present in industrial effluent gas streams (fumes). As such, technologies that aim to convert CO₂ immediately at the exit of industrial installations, could take advantage of this major and unavoidable “contaminant”. Several routes for the combined conversion of CO₂ and H₂O have already reported promising results, e.g. thermochemical, electrochemical, and photochemical, either with or without catalysts, and all their possible combinations.^[2,6–11] In recent years, another technology considered to have potential in this area is (non-thermal) plasma.^[12–14]

The main advantage of (non-thermal) plasma is that the gas can remain near room temperature while being “activated” by electron impact excitation, ionization and dissociation reactions. Furthermore, non-thermal plasmas do not suffer from several disadvantages of existing technologies, like using expensive or scarce materials, the large size of the systems, inefficient energy input for heating of the systems, or short durability of the electrodes. Instead it is a flexible, so called “key-turn”, process operated by a power source and the desired gas mixture, and it can be built with durable inexpensive materials.^[15]

Just like electrochemical techniques, plasma technology uses electricity as an energy source. As such it can also provide a solution for the imbalance between energy production and consumption by intermittent renewable sources, e.g. solar and wind. Taking all the above into account, and especially the fact that plasma is an instantaneous “on-and-off” technique that can use renewable energy sources when they are available, makes plasma an inherent “green” technology. In this scenario the electrical energy can be stored in a chemical form. The reactions of greatest interest are the conversion of CO₂ to syngas, hydrocarbons, short-chain olefins (ethylene and propylene) and oxygenated products (i.e. methanol, formaldehyde, dimethyl ether, formic acid, hydrogen peroxide, etc.). For most applications, liquids would be preferable to gases, since they have much higher energy densities (both gravimetric as volumetric) than electrical

[a] Title(s), Initial(s), Surname(s) of Author(s) including Corresponding Author(s): MSc Ramses Snoeckx, Prof. dr. Annemie Bogaerts
Department: Department of Chemistry, research group PLASMANT
Institution: University of Antwerp
Address 1: Universiteitsplein 1, 2610 Antwerp, Belgium
E-mail: Ramses.snoeckx@uantwerpen.be

[b] Title(s), Initial(s), Surname(s) of Author(s): MSc Alp Ozkan, Prof. Dr. Francois Reniers
Department: Chimie analytique et chimie des interfaces
Institution: Université Libre de Bruxelles
Address 2: Campus de la Plaine, Bâtiment A, CP255, boulevard du Triomphe, 1050 Bruxelles

Supporting information for this article is given via a link at the end of the document.

storage techniques.^[16,17] Nevertheless, syngas can easily be converted to almost any commercial bulk chemical or fuel through the Fischer Tropsch synthesis.^[18] For this purpose, it is of great importance to have a high sense of control over the H₂/CO ratio to be able to steer the synthesis towards the desired products.^[19] Other products of interest that can in principle be formed starting from CO₂ and H₂O are peroxides. Hydrogen peroxide (H₂O₂) has been shown to be a microbicidal active agent and its ability to sterilize is widely used and well-studied.^[20–22] As such, the production of H₂O₂ by plasma technology is gaining a lot of interest for biomedical and (bio-)decontamination applications.^[23–25] In a recent extensive review by Lu et al., which focuses on the generation, transport and biological effects of the reactive plasma species, H₂O₂ is even considered to be one of the most important reactive oxygen species that acts as signaling molecule, together with O₂⁻.^[26]

Before explaining the experimental setup and the model, we will give a brief overview on the current state-of-the-art of plasma-based combined CO₂ and H₂O conversion, to highlight the main trends observed until now and also to identify the current knowledge gap with respect to the underlying mechanisms. This work aims to fill this knowledge gap, by a combination of experiments and especially computations.

State-Of-The-Art On Plasma-Based Combined CO₂ And H₂O Conversion

Because of its advantages over conventional reforming technologies, a lot of research was already devoted to the plasma-based conversion of greenhouse gases into value added products. Most research was based on pure CO₂ splitting^[27–36] or dry reforming of methane^[12,14,37–50] Pure H₂O plasmas for the production of hydrogen have also been extensively studied.^[51–55] However, the research on the simultaneous conversion of CO₂ and H₂O into syngas or oxygenated products by plasma is very limited. Ihara et al.^[56,57] were the first to investigate the conversion of CO₂ and H₂O, by means of a microwave plasma set-up. Other researchers have considered a ferroelectric packed-bed reactor,^[58] a dielectric barrier discharge (DBD),^[58] a DBD packed with Ni/γ-Al₂O₃ catalyst,^[59] a surface discharge,^[60] a negative DC corona discharge,^[61] and a surface-wave microwave discharge.^[15] In general, five main trends can be distinguished from the above literature:

- The CO₂ conversion increases with increasing energy input;
- The H₂/CO ratio decreases with increasing energy input;
- The CO₂ conversion decreases with increasing water content;
- The H₂/CO ratio increases with increasing water content;
- The main products formed are H₂, CO and O₂, but some papers also report the production of hydrogen peroxide (H₂O₂),^[56] oxalic acid (C₂H₂O₄),^[56] formic acid (CH₂O₂),^[60] methane (CH₄),^[59,60] dimethyl ether (C₂H₆O, DME),^[60] methanol (CH₃OH)^[57,59,61] and ethanol (C₂H₅OH).^[61] Unfortunately, most data on the formation of these products are only qualitative and incomplete, making it

impossible to deduce a general trend on product yields or selectivities.

It becomes clear that not much is known about the simultaneous conversion of CO₂ and H₂O into value added products, and specifically not about the underlying mechanisms. In this paper, we study the combined plasma-based conversion of CO₂ and H₂O for a DBD plasma reactor, by means of experiments and computer simulations, based on a zero-dimensional (0D) chemical kinetics model.

The main aim of this study is to evaluate whether the combined conversion of CO₂ and H₂O using plasma can become a viable route to produce value-added chemicals, by identifying and analyzing the underlying plasma chemical kinetic behavior. For this analysis, first a plasma chemical kinetics model for CO₂/H₂O and its interactions needs to be developed. The investigation will then be performed in a step-wise manner, by first determining the influence of the water content and the SEI on the conversion and product formation in a combined effort of experiments and computations. The latter also allows to validate the model. Subsequently, a detailed chemical kinetics analysis will be performed to elucidate the mechanisms behind the observed trends. This approach enables us to investigate the current and future possibilities and limitations in more detail. Furthermore, based on this analysis we can also suggest possible solutions to enhance the formation of the desired products, and as such, make an initial evaluation towards the industrial viability of plasma technology for this process.

Results And Discussion

First we will compare the measured conversion of CO₂ and H₂O and the product selectivities with the model calculations. We will also discuss in detail the underlying chemistry for the obtained results, based on the model predictions, to explain the observed trends. Subsequently, we will briefly discuss additional simulations for a broader range of conditions, to predict the CO₂ and H₂O conversion, and the product selectivities, at larger values of SEI and water contents. Finally, based on this plasma chemical kinetic analysis, we will summarize the current potential and limitations of plasma technology for combined CO₂ and H₂O conversion into value added chemicals, and propose some solutions on how to move forward in this field.

Conversion And Selectivity: A Comparison Between Experiments And Model Calculations

CO₂ And H₂O Conversion

In Figure 1 the experimental and calculated absolute CO₂ and H₂O conversions are plotted as a function of water vapor content for a total gas flow rate of 600 mL/min at 323 K, for three different SEI values, i.e., 3.2, 4.0 and 4.8 J/cm³. As to be expected, the absolute CO₂ and H₂O conversions increase when more energy is supplied, i.e. at higher SEI values. Regardless of the SEI, both the experimental and calculated absolute CO₂ conversion is the highest for pure CO₂, when no water vapor is added to the discharge. The experimental conversions in this case are 4.3, 3.3

and 2.6 % for the three different SEI values investigated, and the calculated values are very similar.

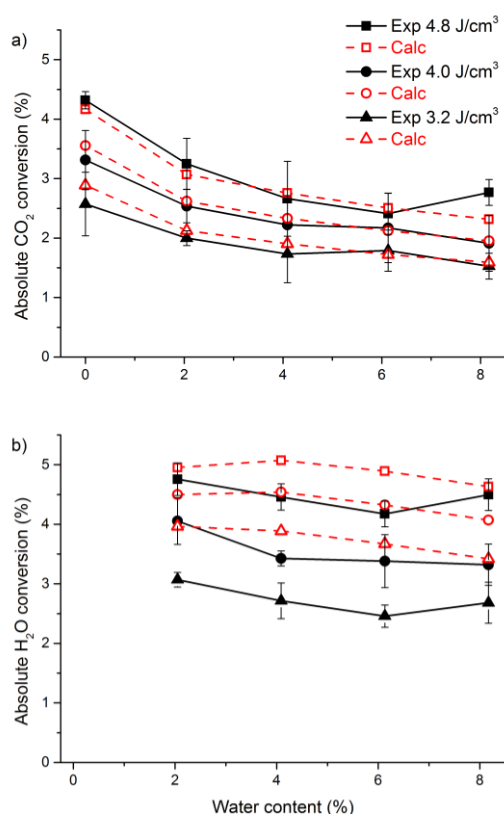


Figure 1. Experimental and calculated values of absolute CO₂ (a) and H₂O (b) conversion as a function of water vapor content for the different values of SEI and a total flow rate of 600 mL/min at 323 K.

The drop in CO₂ conversion with increasing water content may result from the destabilization of the discharge induced by the presence of water. Indeed, our calculations reveal a ~ 40 % drop of the maximum electron density with increasing water content from 0 to 8 %. Furthermore, our chemical analysis pathway also allows us to identify a chemical reason for the drop in CO₂ conversion, as will be explained in the underlying mechanism section below. Adding 2 % water vapor yields a drop in the CO₂ conversion by about 25 % for all SEI values investigated. When increasing the water content up to 8 %, the CO₂ conversion continues to drop slightly by an additional 15–25 %, compared to the conversion at 2 % water, and depending on the SEI. As the CO₂ content in the gas flow drops upon increasing H₂O fraction, the effective CO₂ conversion will drop even more than the absolute CO₂ conversion, i.e., from 4.3–2.6 % (depending on the SEI, see above) for pure CO₂, till 2.5–1.4 %, for 8 % H₂O addition (see ESI, Figure S3).

The absolute H₂O conversion shows a slightly decreasing trend of about 10 % with increasing water content from 2 to 8 %. At a water content of 2 % the absolute experimental H₂O conversions are 4.8, 4.1 and 3.1 %, for an SEI of 4.8, 4.0 and 3.2 J/cm³,

respectively, while these values amount to 4.5, 3.3 and 2.7 % at a water content of 8 %. As the drop in absolute H₂O conversion is limited, the effective H₂O conversion obviously rises upon higher water content (from 2 to 8 %), i.e., from 0.10 to 0.37 %, from 0.08 to 0.27 % and from 0.06 to 0.22 %, for an SEI of 4.8, 4.0 and 3.2 J/cm³, respectively (see ESI, Figure S3).

The calculated H₂O conversions are overestimated, on average by about 9.5, 23.5 and 37.3 % in the entire range of water addition, for the SEI values of 4.8, 4.0 and 3.2 J/cm³, respectively, compared to the experimental values. This overestimation is probably due to some more complex processes taking place in the experiments as a result of the water vapor, which could not be easily accounted for in the 0D plasma chemistry model. Indeed, the model describes all chemical processes, but does not take into account some physical effects, such as condensation and nebulization. It is well possible that the evaporation in reality is not complete, leading to small droplets (nebulization) of water spread throughout the discharge zone, despite the fact that the entire plasma system is heated starting from the CEM. This would lead to a lower concentration of gaseous H₂O that can undergo reactions in the plasma, but nevertheless this H₂O will also reach the MS capillary and thus will be accounted for when calculating the conversion (cf. Equation 2 above). Hence, this results in a lower experimental conversion. Upon increasing the SEI, more energy is supplied to the gas and slightly more heat is locally generated in the discharge filaments, which might reduce the probability of condensation, and this may explain the lower deviation between calculated and measured conversion with increasing SEI values.

Product Selectivity

CO₂ splitting typically yields CO and O₂ molecules, the latter being formed by the recombination of O atoms. Besides, also some O₃ can be created.^[28] Upon addition of a H-source, such as CH₄ or H₂O, we target the production of small oxygenated hydrocarbons, such as formaldehyde, methanol and formic acid. In the case of CH₄ addition in the plasma, we mainly form syngas, as demonstrated before.^[62] In the present paper, we investigate whether H₂O addition to a DBD plasma can result in some oxygenated molecules, like reported for microwave, atmospheric surface and negative DC corona discharge plasmas^[56,57,60,61]; see the state-of-the-art above. Unfortunately, for all investigated cases in both the experiments and calculations, the main products formed are O₂, and the syngas components CO and H₂. We do form some hydrogen peroxide (H₂O₂) and trace amounts of ozone (O₃), but no oxygenated hydrocarbons were detected in the experiments, and the calculated concentrations of methanol and formaldehyde were only in the ppb range (hence far below the experimental detection level). The reason for this will be discussed in more detail in the next section, by elucidating the underlying chemistry.

Figure 2 represents the calculated number densities of the most important molecules present or formed in the plasma, as a function of time for an SEI of 4 J/cm³ and a water content of 4 %. The total residence time of the gas in the plasma reactor corresponds to 1.66 s, as indicated above. The CO₂ and H₂O density show a slightly decreasing trend, in line with their

conversion. As a consequence, the main products formed, i.e., CO, O₂, H₂ (and O₃), exhibit the opposite increasing trend, with final concentrations in the percentage range (see also below). H₂O₂ is characterized by a slightly different, more flat trend, with final concentration in the ppm range. Finally, the oxygenated products (CH₂O and CH₃OH), together with CH₄, reach concentrations well below the ppm range.

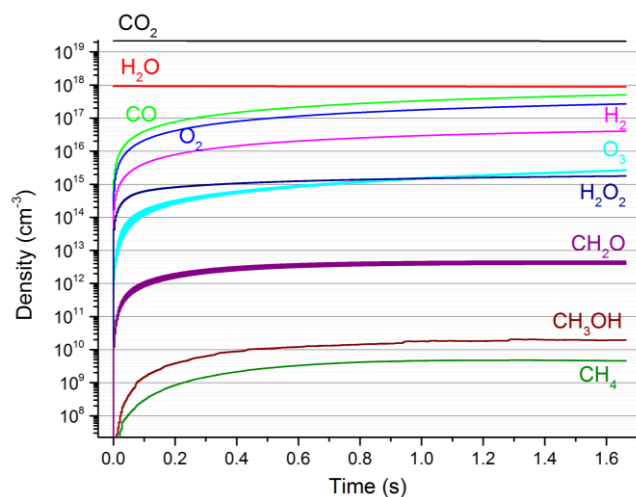


Figure 2. Calculated species densities of the most important molecules present or formed in the plasma, as a function of time for an SEI of 4 J/cm³ and a water content of 4 %.

Table 1. Measured and calculated gas composition after plasma treatment for an SEI of 4.0 J/cm³, and for the different water vapor contents investigated, with the remainder being unconverted CO₂ and H₂O.

Water content [%]	O ₂ [%]	CO [%]	H ₂ [%]	H ₂ O ₂ [ppm]	O ₃ [ppm]
2.05 (Exp)	1.27 ± 0.11	2.46 ± 0.32	0.081 ± 0.006	ca. 10–100	ca. 10
2.05 (Calc)	1.28	2.53	0.09	47	193
4.09 (Exp)	1.12 ± 0.18	2.11 ± 0.53	0.138 ± 0.015	ca. 10–100	ca. 10
4.09 (Calc)	1.17	2.21	0.18	77	118
6.13 (Exp)	1.11 ± 0.13	2.02 ± 0.27	0.205 ± 0.005	ca. 10–100	ca. 10
6.13 (Calc)	1.09	1.97	0.25	106	96
8.17 (Exp)	1.00 ± 0.08	1.74 ± 0.14	0.269 ± 0.003	ca. 10–100	ca. 10
8.17 (Calc)	1.03	1.77	0.32	135	81

The measured and calculated concentrations of O₂, CO, H₂, H₂O₂ and O₃ are listed in Table 1, for the different water vapour contents investigated, and for an SEI of 4.0 J/cm³. The results for the other SEI values can be found in the ESI.

The agreement between measured and calculated gas composition is very good. CO is the main product, as expected (due to the higher CO₂ content in the mixture), but its fraction obviously drops upon increasing H₂O content, as is also the case for the O₂ and O₃ fraction. The H₂ and H₂O₂ fractions, on the other hand, rise upon addition of more H₂O, which is also logical. The O₃ and H₂O₂ contents could—although detected—not be quantified, due to their low signal-to-noise ratio, so only an order of magnitude could be given for the experimental data in Table 1. If we take a look at the experimental and calculated H₂/CO ratio (also known as syngas ratio) in Figure 3, we can draw the following conclusions. First of all, the calculated ratios are higher than the experimental values. This is of course a direct result of the above mentioned overestimation of the H₂O conversion, which leads to a higher concentration of H₂.

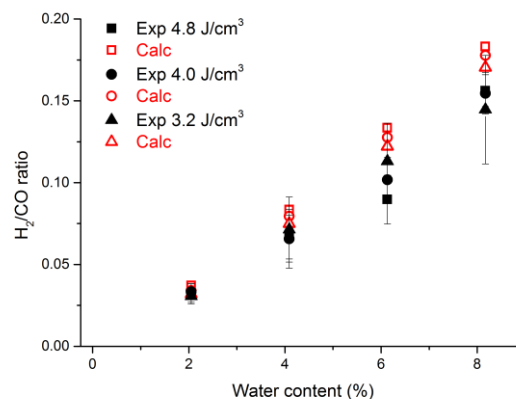


Figure 3. Experimental and calculated values of H₂/CO ratio as a function of water vapor content for the different values of SEI and a total flow rate of 600 mL/min at 323 K.

Secondly, the SEI has only a minor effect on the syngas ratio in the investigated range. Finally, and most importantly, the H₂/CO ratio increases linearly with increasing water content. This is logical because the absolute H₂O and CO₂ conversions only decrease slightly upon increasing water content (see above), so a higher water content (and thus a lower CO₂ content) leads to an increase in the effective production of H₂ (being formed out of H₂O) and a drop in CO production (being formed out of CO₂). As such, although no detectable amounts of oxygenated hydrocarbons are produced, this type of combined CO₂ and H₂O plasma conversion could still be of significant interest, because changing the water content in the gas mixture allows for a process with an easily controllable H₂/CO ratio. This is very important, since several post-processes require a different syngas ratio depending on the targeted products.^[19] For example, Fischer Tropsch synthesis needs a ratio of 1.7 or 2.15, depending on the catalyst used, while for methanol synthesis a ratio of 3 is needed. The values obtained here, i.e., for water vapor contents up to 8 %, are in the range of 0.03 to 0.18.

lead to syngas ratios clearly below 1, and thus they will need hydrogen enrichment for most practical applications. However, further in this paper we will investigate the conversion process in a wider range of water vapor contents and SEI values, yielding significantly larger syngas ratios up to 8.6 (see below). Figure 4 illustrates the measured and calculated O-based selectivity of CO and O₂ and H-based selectivity of H₂ and H₂O₂ as a function of the water vapor content. The results are only shown for an SEI of 3.2 J/cm³, since the absolute values and especially the trends of the selectivities appear to be almost independent from the used SEI, and the data at the other SEI values can be found in the ESI.

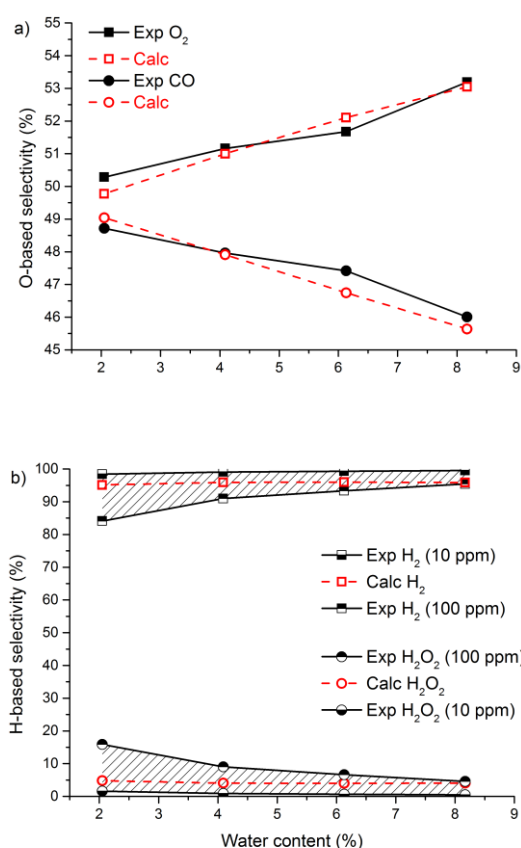


Figure 4. Experimental and calculated values of O-based (a) and H-based (b) selectivity of the major products as a function of water vapor content for a SEI value of 3.2 J/cm³ and a total flow rate of 600 mL/min at 323 K. Note that although H₂O₂ was detected during the measurements (ca. 10–100 ppm), it could not be exactly quantified due to its low signal-to-noise ratio; therefore, a selectivity range is presented for the experimental H-based selectivities.

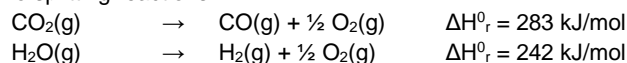
The O-based selectivity in Figure 4(a) indicates that with increasing water content from 2 to 8%, the experimental O₂ selectivity increases from 50.3 to 53.2 % and the CO selectivity decreases from 48.7 to 46 %. The calculated values are in excellent agreement with the measured values (note the detailed

Y-axis). The rise in O₂ selectivity upon increasing water content can easily be explained by the conversion of H₂O which leads to the additional formation of O₂ and thus increased selectivity for O₂ and decreased selectivity for CO. The sum of the CO and O₂ selectivity is about 99 %. The remaining 1 % selectivity in both the experimental and calculated results is accounted for by O₃ and H₂O₂.

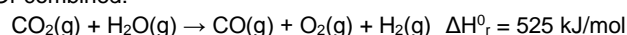
Figure 4(b) shows the H-based selectivity versus the water content. The calculated H₂ selectivity is about 95 - 96 % and the remaining 4–5 % is due to the selectivity towards H₂O₂, independent of the water content within the investigated range. Although it is clear from the MS spectra that H₂O₂ is present in the mixture, its signal-to-noise ratio is too low to exactly quantify its effective amount and hence to calculate its selectivity directly. Nevertheless, from the spectra it was possible to estimate its concentration to be in the order of 10–100 ppm. Since the calculated selectivity for H₂O₂ corresponds to a concentration between 47 and 135 ppm (cf. Table 1 above), this is indeed in the same range as the measured values. We calculated the experimental selectivity for H₂ and H₂O₂ for this range of 10-100 ppm, taking these values as lower and upper limit, respectively; see shaded area in Figure 4(b). As to be expected, for low water contents the calculated results are closer to the values for 10 ppm, while at higher water contents the values are closer to the values of 100 ppm, since our calculations predict an increase of H₂O₂ with increasing water content. From these results we may conclude that all calculated selectivity results are in good agreement with the experiments.

Energy Efficiency

Since the main products are CO, O₂ and H₂, the energy efficiency can be based on the standard reaction enthalpies of the following two splitting reactions:



Or combined:



As such, we can calculate the energy efficiency for our process by the following formula:

$$\eta = \frac{X_{eff,CO_2} \cdot 283 \left(\frac{\text{kJ}}{\text{mol}}\right) + X_{eff,H_2O} \cdot 242 \left(\frac{\text{kJ}}{\text{mol}}\right)}{SEI \left(\frac{\text{kJ}}{\text{mol}}\right)} \quad [\text{Eq.}(1)]$$

The values for the energy efficiencies obtained in this way, both in the experiments and calculations, are presented in Table 2.

For pure CO₂ splitting the thermal equilibrium dissociation limit lies at about 60 % energy efficiency and the same target is assumed for dry reforming of methane.^[62–64] At the same time the energy efficiency of water splitting by electrolysis lies in the same 60–70 % range. Therefore, we believe that the same 60 % energy efficiency should be the target for the combined process under study here. If we do not take the energy into account required for evaporating the water and heating the system, the highest (measured) energy efficiency achieved in our study is 7.3 %, for an SEI of 4.8 J/cm³ and a water content of 2.05 %. As such, it becomes clear that from an energetic point of view the process needs to be improved by at least a factor 8 to be considered

competitive. It should be realized, however, that by adding a catalyst, which we believe is necessary to target the production of value-added compounds like methanol, the energy efficiency of a DBD plasma reactor typically also improves. In most cases, the catalyst is added as beads or pellets in a DBD reactor, yielding a so-called packed-bed DBD, which gives rise to electric field enhancements near the contact points of the beads or pellets,^[65] leading to higher electron energies, and thus more pronounced electron impact dissociation of the gas molecules for the same applied power, resulting in a better energy efficiency. The latter was indeed demonstrated in several papers for pure CO₂ splitting,^[66–68] and we believe that similar improvements in energy efficiency would also be possible for the combined CO₂/H₂O conversion.

Table 2. Experimental and calculated energy efficiencies based on the standard reaction enthalpy, for the different specific energy inputs and water vapor contents investigated.

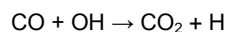
SEI (J/cm ³)	Water content (%)	η (exp) (%)	η (calc) (%)
3.2	2.05	6.7	7.2
	4.09	5.9	6.5
	6.13	6.0	6.0
	8.17	5.3	5.7
4.0	2.05	6.8	7.1
	4.09	6.0	6.4
	6.13	5.9	5.9
	8.17	5.3	5.5
4.08	2.05	7.3	6.9
	4.09	6.0	6.3
	6.13	5.5	5.8
	8.17	6.4	5.5

Underlying Mechanisms For The Observed Trends.

As shown above, the experiments and computer simulations reveal exactly the same trends for the absolute conversion of CO₂ and H₂O and for the selectivity towards CO, H₂ and O₂. This justifies using the plasma chemistry model for the most important—and chemically most interesting part—of this work, i.e., analyzing the main reactions taking place, to describe and explain the observed macroscopic trends, and eventually to compile a general reaction scheme, which illustrates the overall underlying chemical reaction mechanisms. This allows us in the end to draw important conclusions, regarding the applicability of this process.

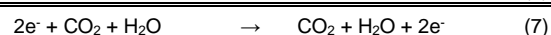
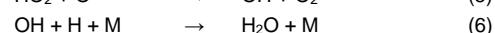
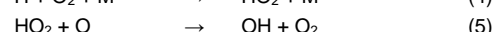
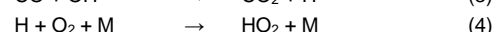
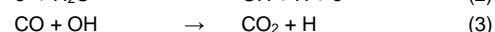
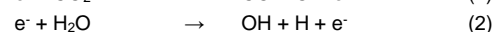
(A) Limited CO₂ (And H₂O) Conversion Upon Water Addition

There are two main reasons why the CO₂ conversion decreases when adding water: a physical reason and a chemical reason. The physical reason was already mentioned above, namely the drop in maximum electron density, which leads to a lower rate of the electron impact dissociation reactions. The chemical reason behind the drop in CO₂ conversion upon rising water vapor content is revealed by the kinetic analysis. One of the crucial reactions for this process is the reaction between CO and OH:



$$k = 5.4 \times 10^{-14} [\text{cm}^3/\text{molecule s}] (T/298 \text{ K})^{1.50} e^{250 [\text{K}]/T}$$

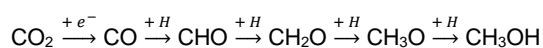
This is a fast reaction and plays a pivotal role in the ratio between the conversion of CO₂ and H₂O. We can explain this in a very simple way by means of the following reaction paths that take place:



Reactions (1) and (2) lead to the (electron impact) dissociation of CO₂ and H₂O, yielding the products CO and OH (as well as O and H atoms). However, due to the large reaction rate constant of reaction (3), CO and OH will quickly recombine to form again CO₂. In these three reactions, two H atoms and one O atom are formed, but they recombine quickly as well, first into OH through the subsequent reactions (4) and (5), and subsequently OH reacts even faster with H back into H₂O through reaction (6). In the end, this leaves us exactly where we started (see overall reaction (7)). Of course, this does not mean that there will be no net conversion of CO₂ and H₂O. Indeed, this is not the only pathway taking place for the conversion of CO₂ and H₂O, but this pathway highlights the interaction between the CO₂ and H₂O dissociation products, which limits their conversion. The overall CO₂ and H₂O loss rates, however, are higher than their formation rates, effectively leading to the observed conversions. Nevertheless, reactions (2) and (3) illustrate why the absolute conversion of CO₂ decreases upon addition of H₂O, while in general an increasing trend is found for the absolute CO₂ conversion in admixtures, i.e. upon addition of N₂,^[69] He^[70,71] and Ar.^[71]

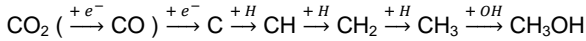
(B) Absence Of Methanol Production

The above reaction scheme can also explain why no production of methanol is observed. Indeed, in 1988 Eliasson et al.^[72] investigated the production of methanol in a CO₂/H₂ DBD reactor. When using the plasma only set-up, the CO₂ conversion reached 12.4 % and the major products were CO (with a selectivity of 96 %) and H₂O, while very small yields of CH₄ and methanol were detected, with selectivities of 3.2 and 0.4 %, respectively. The authors proposed the following radical reaction mechanism for the formation of methanol:



These reactions are also included in our model, but they seem to be of minor importance when using H₂O as a co-reactant, because the H atoms are quickly consumed by O₂ and OH, according to the scheme presented above (reactions (4) and (6)). Our plasma chemistry model elucidates that in the case of a CO₂/H₂O mixture another pathway to methanol is more important (note that the reactant "+H" above the arrows does not only

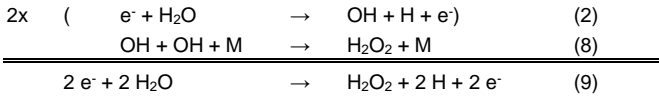
designate H atoms but can also be replaced by other H-containing species such as H₂, HO₂, H₂O, ...):



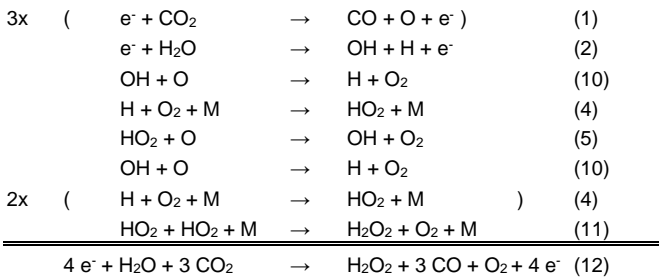
Nevertheless, both these pathways turn out to be unimportant in our case, because the H atoms that are needed to start forming CHO and CH fragments from CO and C, respectively, are being steered to OH and subsequently to H₂O again (see reactions (4-6) above), leaving no room for the production of oxygenated hydrocarbons, such as methanol. This chemical analysis reveals that H₂O might not be a suitable H-source for the formation of methanol (as well as other oxygenated hydrocarbons) after all, because of the abundance of O atoms, O₂ molecules and OH radicals, trapping the H atoms. This important new insight will allow us to propose solutions on how the production of methanol might still be pursued in a CO₂/H₂O plasma and/or which other options might be more attractive, as will be elaborated in the Summary below.

(C) Formation Of H₂O₂

Both our experiments and calculations illustrate that a mixture of CO₂ and H₂O can yield non-negligible amounts of H₂O₂, which is also of great value, more specifically for decontamination purposes, as explained in the Introduction. The main pathways for the production of H₂O₂, as revealed by our chemical kinetics analysis, are:



Reaction (2) leads to the (electron impact) dissociation of H₂O into H and OH. Subsequently, 2 OH radicals react with each other in the presence of a third body, to form H₂O₂ (reaction (8)). For the operating conditions investigated here, i.e., water contents up to 8 % and SEI values up to 4.8 J/cm³, this pathway is responsible for 90 % of the H₂O₂ production. The remaining 10 % follows a slightly more complicated pathway:



Reactions (1) and (2) again lead to the (electron impact) dissociation of CO₂ and H₂O, producing CO, O, OH and H. OH and O subsequently form H and O₂ (reaction (10)), which then react further with a third body to HO₂ (reaction (4)). HO₂ turns out to be the main production source for O₂ and the second most important source for OH (reaction (5)). Next, reactions (11) and (4) can repeat themselves, finally yielding two HO₂ radicals, which

react with each other in a three-body reaction, producing H₂O₂ and O₂ (11). Thus, the overall reaction is given by reaction (12).

(D) General Reaction Overview

A general reaction overview is illustrated in Figure 5, which is composed of the time-integrated formation and loss rates of the most important species in our model for explaining the chemical pathways taking place. The results are presented for an SEI of 3.2 J/cm³ and 8 % water content. A higher SEI yields higher integrated rates, but does not change the reaction paths significantly. A lower water content only decreases the reaction rates of the H₂O chemistry but again, it does not change the reaction paths significantly.

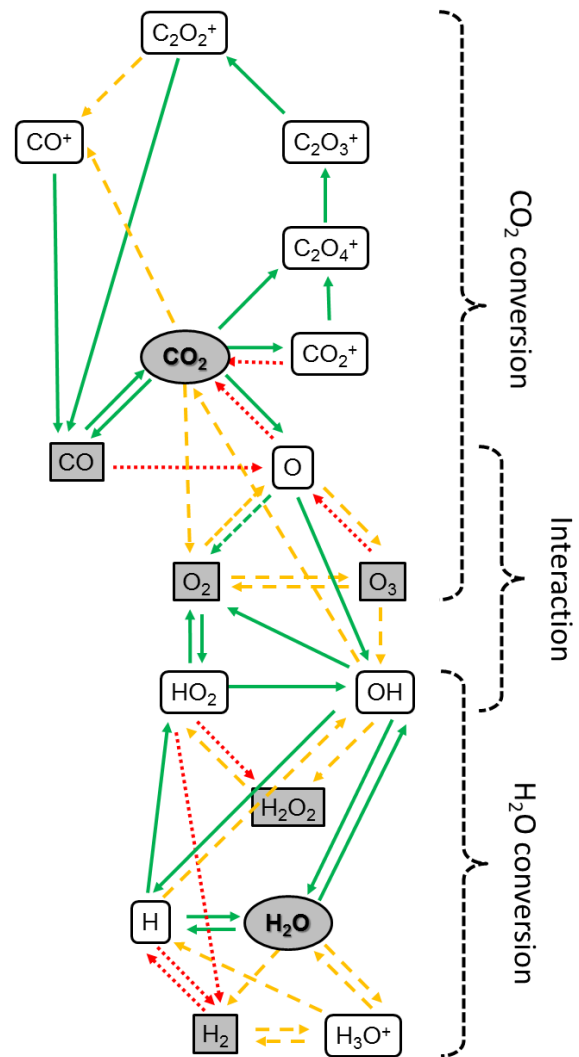
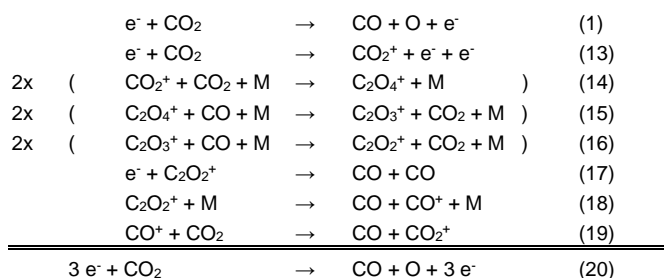
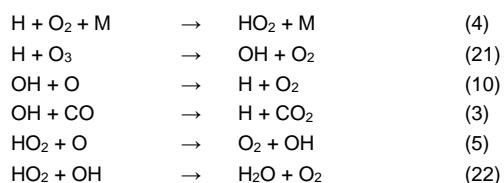


Figure 5. Reaction scheme to illustrate the main pathways for CO₂ and H₂O conversion and their interactions. The arrow lines represent the formation rates of the species, with full green lines being formation rates over 10¹⁷ cm⁻³.s⁻¹, orange dashed lines between 10¹⁷ and 10¹⁶ cm⁻³.s⁻¹ and red dotted lines between 10¹⁶ and 10¹⁵ cm⁻³.s⁻¹.

The reaction scheme can be divided in three main parts: the top part describes the CO₂ conversion, the bottom part deals with the H₂O conversion and the middle part explains the interaction between both. The arrow lines represent the formation rates of the species they point to, with full green lines being formation rates over 10¹⁷ cm⁻³·s⁻¹, orange dashed lines between 10¹⁷ and 10¹⁶ cm⁻³·s⁻¹ and red dotted lines between 10¹⁶ and 10¹⁵ cm⁻³·s⁻¹. Starting from CO₂ the main reactions are electron impact dissociation towards CO and O, and electron impact ionization towards CO₂⁺. Once ionization takes place, the main reaction path becomes CO₂⁺ + CO₂ + M → C₂O₄⁺ + M (reaction (14) below). The C₂O₄⁺ ions convert further into C₂O₃⁺ and C₂O₂⁺ ions (reactions (15) and (16) below), and the latter ions split into two CO molecules or into CO and CO⁺ (reactions (17) and (18) below). The CO molecules are mainly consumed in these ion conversion processes, forming again CO₂. Thus, a circular pathway interaction between CO and CO₂ takes place, as illustrated by reactions (13)-(19) below, with no net conversion. The only net conversion is due to electron impact dissociation (reaction (1)). This can be summarized as follows:



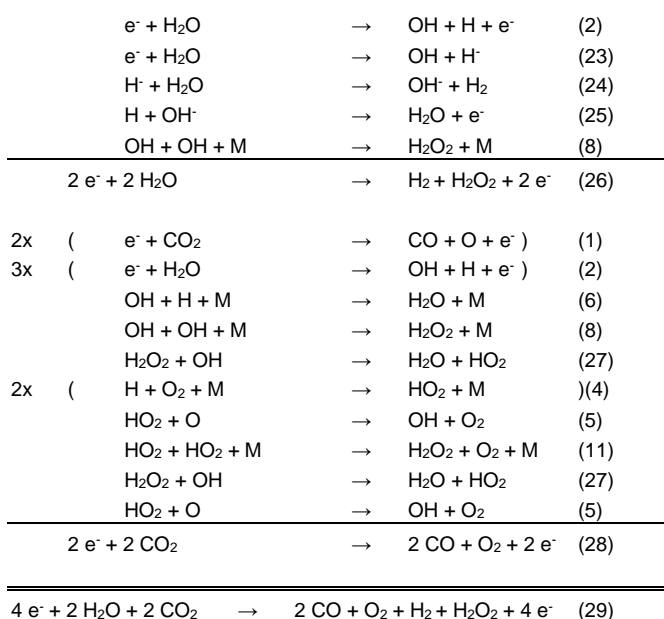
Furthermore, the O atoms formed by the CO₂ splitting are also involved in a triangular interaction with O₂ and O₃, as already described in our earlier work,^[28,69] with the main product being O₂. Thus, the two main products of CO₂ splitting are CO and O₂. The interaction between CO₂ and H₂O takes place through the intermediate water products (H, OH and HO₂) with O, O₂, O₃ and CO, through the following main reactions:



Starting from H₂O the main reaction is also electron impact dissociation into OH and H (see reaction (2)). Other products formed are H₂ (mainly through reactions (23) and (24) below) and intermediate ions such as H₃O⁺ (not included in the reactions below). Although the formation rates of H₂ are only moderate, its loss rates are even lower, explaining why it is still one of the main reaction products. The main reaction for OH and H radicals is their recombination into H₂O (see reaction (6) below). Moreover, part of the OH radicals also recombine into H₂O₂ through a third body reaction (see reaction (8)). This reaction is indeed the main production pathway for hydrogen peroxide, as explained above.

In turn, H₂O₂ can be destroyed upon reaction with an additional OH radical (see reaction (27)). Just like for O, O₂ and O₃, an interaction is taking place between OH, HO₂ and H₂O₂, which can be summarized as follows: HO₂, mainly formed from H and O₂ (reaction (4)), reacts with O to form OH (reaction (5)). As explained above, HO₂ can also recombine to form H₂O₂ (reaction (11)) and again part of this H₂O₂ is converted back into HO₂ (reaction (27)).

If we combine the net reactions (26) and (28), we get the overall reaction (29), which is one of the most important reaction paths of the conversion of CO₂ and H₂O in the main observed products O₂, CO, H₂ and H₂O₂.



Model Predictions In A Wider Range

So far our experiments and modelling calculations are perfectly in line with four of the five main observations from literature (see end of the State-of-the-art Section): (i) the CO₂ conversion increases with increasing energy input; (ii) the CO₂ conversion drops with increasing water content; (iii) the H₂/CO ratio increases with increasing water content; and (iv) the main products formed are H₂, CO, O₂ and (ppm amounts of) H₂O₂.

Nevertheless, the above study could only be carried out for a small range of experimental conditions, based on the available set up. To analyze this process for a wider range of conditions and especially to reveal whether the latter can yield certain products in larger amounts, we have performed additional model calculations, beyond what is typically accessible for one experimental set up. More specifically, we have varied the SEI from 5 to 250 J/cm³ for water contents from 10 to 90 %.

Since this newly developed chemistry model was not validated in this wider range of conditions, caution is advised with its interpretation and predictive value. Another critical note is that the experimental conditions required to achieve the highest water contents under study might not be straightforward to realize, due to the condensation issues already observed at low

concentrations. One solution might, therefore, be to dilute the entire mixture with an inert gas, such as argon or helium. Nitrogen is probably less suited, since it gives rise to NO_x formation.^[69] This approach would also solve possible safety issues, but on the other hand, increase the energy cost, as discussed in the Summary section below.

Although caution is advised when extrapolating models outside their validated range, our previous modelling studies^[14,28,62,69,73] for several different mixtures have already shown that in general the plasma chemistry behavior is almost independent of the SEI, showing a steadily increasing trend of conversion and production. The same studies with admixtures have also shown that in general the plasma chemistry follows a stable and logic trend when changing the mixture ratios. Furthermore, we performed a sensitivity analysis for the most important reactions, which showed that when taking the uncertainties of the reaction rate constants into account, the average deviation on the calculation results is indeed independent of the SEI and only ca. 2 % on average (see ESI for more details). Hence, extrapolation of the model to a wider range of conditions would give us the opportunity to investigate whether the same results can be expected in this wider range, and/or whether certain products can be formed in larger amounts, and thus, give an indication whether it would be worth pursuing these other conditions experimentally. Below, the obtained results will be briefly summarized, but more details can be found in the ESI.

The absolute CO_2 conversion (see ESI, Figure S7(a)) shows the same trends as observed before: it increases with increasing SEI, and it drops with increasing water content over the entire range, with the initial drop being most pronounced. The absolute H_2O conversion, on the other hand, shows different trends depending on the SEI, i.e., it either drops or rises with increasing water content, at low or high SEI values (see ESI, Figure S7(b)). Furthermore, at low water contents, it now drops with increasing SEI. This clearly indicates that the CO_2 chemistry shows mainly the same behavior as presented above, while the H_2O chemistry changes with increasing SEI and water content.

The main products are again O_2 and the syngas components CO and H_2 , while the oxygenated hydrocarbons are again not formed in concentrations above 20 ppm. However, the production of H_2O_2 increases significantly with increasing SEI and water content, and concentrations in the range of 300 ppm to 2.2 % are achieved (see Tables in ESI, section 2.2.2.). The same logical trends upon increasing water content as in Table 1 above are also observed, i.e., a drop for the O_2 , CO and O_3 concentrations and a rise for the H_2 and H_2O_2 concentrations. The H_2 concentration increases significantly upon addition of more water, and becomes clearly larger than CO for the highest water contents. This has a beneficial effect for the H_2/CO ratio, which increases drastically with water content (see ESI, Figure S9). Moreover, it drops upon increasing SEI, which is in line with the fifth observation reported in literature.^[15,59] The latter can be explained by the effective H_2O conversion, which starts to saturate with increasing SEI, while the effective CO_2 conversion keeps on rising. The maximum calculated H_2/CO ratio is around 8.6, and is obtained at 5 J/cm^3 and 90 % water content (see ESI, Figure S9). As such, our earlier claim that plasma technology allows for a process with a

controllable H_2/CO ratio is confirmed in this wider range of water contents and SEI values. Our calculations reveal that depending on water content and SEI, a $\text{CO}_2/\text{H}_2\text{O}$ plasma is able to supply a hydrogen-rich syngas ratio for both various direct Fischer Tropsch synthesis processes and methanol synthesis.

The chemical behavior in this extended range can be explained with Figure 5 above. CO_2 is split into CO and O , which will subsequently form O_2 , and there is no "fast" pathway back to CO_2 . H_2O , on the other hand, is split into OH and H , which are both reactive products, and the "fastest" pathway for both is the recombination back to H_2O . Hence, due to Le Chatelier's principle, upon increasing SEI, the CO_2 conversion will keep on rising, since its dissociation products (i.e., O) react away, or are stable molecules (i.e., O_2 and O_3) that do not quickly react back to CO_2 , while for H_2O , an equilibrium between conversion and formation will be reached, explaining why the H_2O conversion reaches a maximum or saturates at a certain SEI value. Even the production of H_2O_2 cannot prevent this, since it is also easily split into OH radicals, leading again to the formation of H_2O .

Summary: Potential And Limitations Of $\text{CO}_2/\text{H}_2\text{O}$ Plasma Conversion

From the above reaction schemes and chemical kinetics analysis, we can draw a number of conclusions. The bad news is that CO_2 and H_2O seem to be unsuitable to create methanol (or other oxygenated hydrocarbons) in a one-step process by means of a DBD plasma. There are too many steps involved in generating CH_3OH in an efficient way, and all of them involve H atoms, which will in our case more quickly recombine with OH into H_2O or with O_2 into HO_2 , which also reacts further with O into OH . This means that we would need to inhibit these two reactions (i.e., both with OH and with O_2). However, even then, the H atoms would more quickly recombine with O atoms into OH . The problem at hand is thus that the interactions of H atoms with oxygen species (either OH , O_3 , O_2 or O atoms) are too fast and their tendency to form H_2O is too strong. This is of course not unexpected since water is one of the end products of total combustion. Although this fast reaction between H and O atoms has already been proven useful in other plasma-based applications (more specifically for O -trapping in the case of CO_2 conversion, providing a solution for the separation of the CO_2 splitting products),^[74] here it plays against us.

On the other hand, our calculations do reveal that a $\text{CO}_2/\text{H}_2\text{O}$ DBD plasma can deliver an easily controllable H_2/CO ratio with a rich hydrogen content, when sufficient amounts of water can be added to the CO_2 plasma. Hence, at first sight it appears suitable to create value-added chemicals, including methanol, in a two-step process, which is good news. However, our calculations also show that the interaction between H_2O and CO_2 dissociation products, i.e., the recombination between OH and CO into CO_2 , and the recombination of H and OH into H_2O , limit the CO_2 and H_2O conversion, and thus the formation of useful products.

Besides syngas, the direct production of sufficient amounts of hydrogen peroxide, which can be used as a disinfectant or for biomedical purposes, seems possible. However, the formation rate of H_2O_2 , is also partially limited by the destruction reaction of

OH + H₂O₂ towards H₂O and HO₂. Therefore, again, the rapid removal of the formed product (i.e., H₂O₂), e.g., by means of a membrane, would be an important aspect for further improving this process.

Based on the reaction pathways outlined above, we believe that, in order to produce value-added chemicals, the plasma should be combined with a catalyst (so-called plasma-catalysis).^[63,75] This catalyst should selectively let the plasma-generated CO and H₂ react into methanol and subsequently separate the methanol from the mixture. For example, Eliasson et al.^[72] used a CuO/ZnO/Al₂O₃ catalyst in a CO₂/H₂ discharge, which led to an increase in methanol yield and selectivity by more than a factor 10. Several other reported catalysts used for the conversion of CO₂ with H₂ might also be interesting to investigate for their suitability in plasma-catalysis, such as Ni-zeolite catalysts for which methanation is reported,^[76] a Rh₁₀/Se catalyst yielding an ethanol selectivity up to 83 %, ^[77] and a Ni-Ga catalyst for the conversion into methanol.^[78] Furthermore, a lot of research into the catalytic CO₂ hydrogenation is showing promising results for CuO/ZnO/ZrO₂, Cu/ZnO-based catalysts promoted with Pd and Ga, Pd/ZnO and Pd/SiO₂ with the addition of Ga.^[79] In general, multicomponent systems (Cu/ZnO/ZrO₂/Al₂O₃/SiO₂) have reported good performances for the formation of methanol starting from CO/CO₂/H₂ mixtures,^[77] making them potentially very interesting for plasma-catalysis, since this is the in-situ generated mixture during plasma-based conversion, as demonstrated in our paper. The additional advantage is that adding a catalyst should also enhance the conversions, due to Le Chatelier's principle. However, it is important to realize that the catalyst affects the discharge and vice versa,^[63,75] so it is recommended to use tailored catalysts for the plasma process rather than simply relying on classical catalysts. As stated by Neyts et al.^[63] it is important to distinguish between physical and chemical effects when introducing a catalyst in a plasma. In this case we are mainly interested in improving the selectivity towards targeted (value-added) products, therefore the focus should be mainly on the chemical effects. This could be done by replacing the stainless steel inner electrode by another metal (e.g., Cu or Ni),^[80] although care should be taken that the contact time between plasma species and catalyst is long enough. For this purpose, adding catalyst pellets in the entire reactor volume, like in a packed bed reactor, might be more suitable. Keeping the reaction scheme and reactive species as predicted by our model in mind, two pathways might be interesting and realistic to achieve: promoting the recombination of OH radicals to H₂O₂ or promoting the reduction of CO to methanol. In both cases the thermodynamic aspects at the nanoscale will become very important, especially since plasma catalysis is a far-from-equilibrium process.^[75] The critical point will be the arrival and binding (e.g., physis- or chemisorption) of the reactants to the catalyst surface. To be successful, this process will have to be faster than the recombination rate of OH with H. Of course, these suggestions are only speculations, and further research will be needed to investigate this in practice.

Note, however, that we need to be cautious about the explosive mixture that might be formed during this process, due to the presence of O₂, together with CO, H₂ and an ignition source in

such a setup. At the research level this will probably never be a problem due to the low volumes and conversions. However, when going to a pilot or industrial scale, with larger volumes and conversions, the risk will increase significantly. Consequently, both the capital and operating costs will increase drastically to ensure safe operations. One way to circumvent this problem is by diluting this mixture with an inert gas, such as argon or helium. In this case, however, an additional separation (for the products) and recuperation (for the inert gas) step will need to be included, which will also increase the cost. Furthermore, part of the input energy will be lost due to the electron impact excitation and ionization of these gases. Therefore, this will reduce the energy efficiency and increase the operating cost, but it ensures safe operations.

Finally, the energy efficiency in a classical DBD reactor is quite limited, i.e., in the order of maximum 10 % for pure CO₂ splitting,^[28] and it will be even lower in the CO₂/H₂O mixture, due to the lower conversion, as indicated in this paper. This again limits the industrial applicability of CO₂/H₂O conversion in a DBD reactor. On the other hand, different plasma reactors, such as microwave or gliding arc plasmas, are characterized by higher energy efficiencies, i.e., in the order of 50%, due to the importance of the CO₂ vibrational kinetics at these conditions.^[33,51] Moreover, they operate at somewhat higher temperatures, i.e., in the order of 1000 K, which enables the addition of more H₂O. Nevertheless, it has been suggested^[35,81] that H₂O might quench the vibrational levels of CO₂, thus reducing the good energy efficiency, characteristic for this type of plasma reactors.

Conclusions

The purpose of this work was to evaluate the viability of plasma technology for the combined conversion of CO₂ and H₂O into value-added products, by obtaining a better understanding of the plasma chemistry, based on a combined experimental and computational study. First a novel plasma chemistry set was developed, based on available data in literature. More importantly, this model was then used to identify and analyze the underlying plasma chemical kinetic behavior, and this allowed us to evaluate whether the combined conversion of CO₂ and H₂O using plasma can become a viable route to produce value-added chemicals. We focused on the effects of the water content and SEI on the H₂O and CO₂ conversion as well as on the formation of products, such as H₂, CO, O₂, H₂O₂ and oxygenated hydrocarbons (i.e. methanol).

We demonstrated that adding a few % of water to a CO₂ plasma in a DBD leads to a steep drop in the CO₂ conversion, and when adding even more water, both the CO₂ and H₂O conversion keep decreasing slightly. Furthermore, as also observed in pure CO₂ and CO₂/CH₄ or CO₂/N₂ mixtures, both the CO₂ and H₂O conversion increase with increasing SEI, resulting from a lower flow rate (or higher residence time) or a higher power. The main products formed are CO, H₂ and O₂, as well as H₂O₂, up to 2 % for high SEI values and water contents.

A detailed kinetic analysis by our model indeed revealed (i) why the CO₂ conversion decreases upon adding water, (ii) why the H₂O conversion is limited, (iii) why no methanol (or other

oxygenated hydrocarbons) formation was observed, and (iv) how H₂O₂ is formed. In general, the main reactive species created in the plasma are OH, CO, O and H. The OH radicals will quickly recombine with CO into CO₂, thereby limiting the CO₂ conversion upon addition of water, while the O and H atoms will undergo reactions to form H₂O again, explaining why the H₂O conversion is also limited. Furthermore, the fast reaction between O/OH and H atoms also explains why no oxygenated products are formed, because it occurs much faster than the possible pathways that might lead to oxygenates.

Since we can elucidate the underlying mechanisms of the limited CO₂ and H₂O conversion and the absence of methanol formation based on our kinetic analysis, this allows us to look for possible solutions to overcome these limitations. However, due to its inherent nature, this mixture seems unsuitable to directly produce methanol in a one-step process using a DBD plasma, unless a suitable catalyst can be found. Furthermore, although plasma technology would allow for a process with an easily steerable syngas ratio—even up to 8.6 according to the extended calculations—making it suitable for Fischer Tropsch synthesis and a two-step process for methanol synthesis, the presence of a highly flammable/explosive mixture makes it doubtful that plasma technology will be the most suitable process for the combined conversion of CO₂ and H₂O on a large industrial scale. One way to solve this problem is to dilute the gas mixture with inert gases, such as argon or helium. The downside, however, is that part of the energy input will be lost to excite and ionize these gases, and an additional separation and recuperation step will need to be added, thus leading to a significant drop in overall energy efficiency.

Experimental Section

Experimental Part

The experiments are carried out in a coaxial DBD reactor (see Figure 6). A stainless steel mesh (ground electrode) is wrapped over the outside of a borosilicate (Pyrex) tube with an outer and inner diameter of 30 and 26 mm, respectively (dielectric thickness = 2 mm). A copper rod with a diameter of 22 mm is placed in the center of the borosilicate tube and used as high voltage electrode. The length of the discharge region is 100 mm with a discharge gap of 2 mm, giving rise to a discharge volume of 15.1 cm³. The DBD is supplied with an AFS generator G10S-V for a maximum power of 1000 W, with a maximum peak-to-peak voltage of 5 kV and frequency of 28.06 kHz. The Q-U Lissajous method^[28,82] is used to calculate the discharge power. The energy input is defined as the specific energy input (SEI), which is equal to the ratio of the calculated discharge power to the gas flow rate:

$$SEI \left(\frac{J}{cm^3} \right) = \frac{\text{Discharge power (W)}}{\text{Flow rate} \left(\frac{ml}{min} \right)} \cdot \frac{60 \left(\frac{s}{min} \right)}{1 \left(\frac{cm^3}{ml} \right)} \quad [\text{Eq. (2)}]$$

Note that the SEI is used here as parameter for the energy input. Normally, it is rather the energy selectivity which is most important, since it defines the fraction of input energy used to drive the reactions, compared to the energy being lost to heating. However, in a DBD there is only local heating due to the discharge filaments. The latter only accounts for a very small fraction of the reactor volume for several nanoseconds, with a repetition in the microseconds scale, yielding a volume-corrected filament frequency of

about 0.01 % per discharge cycle.^[83] Thus overall, the gas heating is very limited, and we can assume that all the energy, as defined by the SEI, goes into driving the reactions. Of course, there are energy losses when converting the (low voltage) outlet power to (high voltage) applied power to discharge power. To-date those may vary greatly depending on the power supply used, but this is independent from the plasma process under study. As such, a lot of (successful) research progress is still being made in minimizing the electrical conversion from outlet power to discharge power.

CO₂ and water vapor are used as feed gases with a continuous total flow rate of 600 mL/min at 323 K, varying the H₂O content in the mixture between 0 and 8 %, resulting in a CO₂ content between 100 and 92 %. The individual CO₂ and water flow rates are controlled via a mass flow controller (Bronkhorst) and a liquid flow controller (Bronkhorst), respectively. Subsequently, both flows are mixed using a controlled evaporator mixer (CEM, Bronkhorst), where both the liquid and the gas flow are heated up in a controlled manner for total evaporation. Finally, this liquid delivery system with vapour control is connected to the DBD reactor. Additionally, the entire system (tubing and reactor) is heated up to 323 K to minimize condensation and to promote total evaporation of the water throughout the discharge, as much as possible.

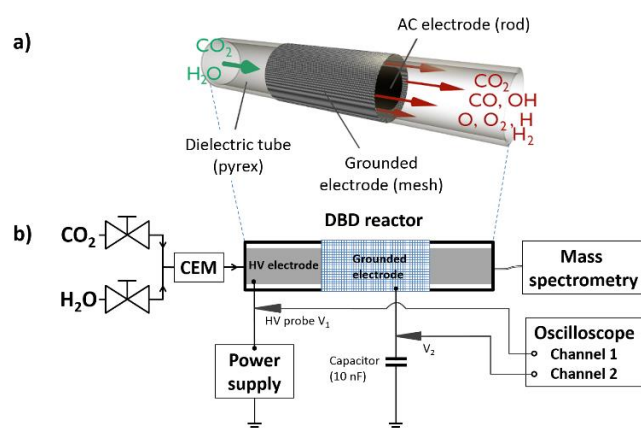


Figure 6. Schematic of the experimental DBD reactor (a) and the experimental setup (b).

The CO₂ and H₂O conversion is studied using mass spectrometry operating at atmospheric pressure (Hiden Analytical QGA MS, Warrington, UK). The multi-level software package MASsoft7 Professional used, allows having a simple control of mass spectrometer parameters. This software also permits to set the electron energy in the ionization chamber at 35 eV or lower for soft ionization in case of complex mixtures, in order to have a reduced spectral fragmentation and simplified data interpretation, for example in case of the presence of more than one reactive component in the discharge. In our case the electron energy in the ionization chamber is set at 35 eV, the detector is a secondary electron multiplier (SEM) and the MASsoft7 software is used to simultaneously monitor the partial pressure variations with specific *m/z* ratios as a function of time. The electrical measurements are performed by means of an oscilloscope (Elektronix DPO 3032) and a high-voltage probe (Tektronix P6015A) in order to evaluate the properties of the discharge. As indicated in Figure 6, the potential V₂ is measured through a capacitor of 10 nF (placed in series with the DBD) to evaluate the power absorbed by the plasma (P_{abs}) via the Lissajous method. This power is used as input in our simulations. Each experiment is repeated three times and the standard deviation is used to express the experimental uncertainties for the presented results. For more details, we refer to the ESI.

The absolute conversion, X_{abs} , of CO_2 and H_2O is calculated from the mass spectrometry response:

$$X_{abs,\text{CO}_2} = \frac{\dot{n}_{\text{CO}_2,\text{inlet}} - \dot{n}_{\text{CO}_2,\text{outlet}}}{\dot{n}_{\text{CO}_2,\text{inlet}}} \quad [\text{Eq. (3)}]$$

$$X_{abs,\text{H}_2\text{O}} = \frac{\dot{n}_{\text{H}_2\text{O},\text{inlet}} - \dot{n}_{\text{H}_2\text{O},\text{outlet}}}{\dot{n}_{\text{H}_2\text{O},\text{inlet}}} \quad [\text{Eq. (4)}]$$

where \dot{n}_i is molar flow rate of species i .

The effective conversion, X_{eff} , is obtained by multiplying the absolute conversion, X_{abs} , with the relative gas content:

$$X_{eff,\text{CO}_2} = X_{abs,\text{CO}_2} \cdot \frac{\dot{n}_{\text{CO}_2,\text{inlet}}}{\dot{n}_{\text{CO}_2,\text{inlet}} + \dot{n}_{\text{H}_2\text{O},\text{inlet}}} \quad [\text{Eq. (5)}]$$

$$X_{eff,\text{H}_2\text{O}} = X_{abs,\text{H}_2\text{O}} \cdot \frac{\dot{n}_{\text{H}_2\text{O},\text{inlet}}}{\dot{n}_{\text{CO}_2,\text{inlet}} + \dot{n}_{\text{H}_2\text{O},\text{inlet}}} \quad [\text{Eq. (6)}]$$

We define here also the effective conversion, along with the absolute conversion, because in plasma research the gas under study is often diluted by helium, argon or nitrogen. Due to this dilution and some energy transfer processes that might occur (e.g., Penning ionization and dissociation), the absolute conversion might increase significantly. However, (a large) part of the input energy is also lost to this dilutant. Therefore, to allow for an easier comparison between diluted and undiluted results, both the absolute and effective conversion are important.

To analyze the products, two different selectivities are defined, i.e., the O-based selectivity for the O-containing species (e.g., O_2 , CO and H_2O_2) and the H-based selectivity for the H-containing species (e.g., H_2 , H_2O_2).

O-based selectivity:

$$S_{\text{O},\text{CO}} = \frac{\dot{n}_{\text{CO},\text{out}}}{2 \cdot [(\dot{n}_{\text{CO}_2,\text{in}} - \dot{n}_{\text{CO}_2,\text{out}}) + 1/2 \cdot (\dot{n}_{\text{H}_2\text{O},\text{in}} - \dot{n}_{\text{H}_2\text{O},\text{out}})]} \quad [\text{Eq. (7)}]$$

$$S_{\text{O},\text{O}_2} = \frac{\dot{n}_{\text{O}_2,\text{out}}}{(\dot{n}_{\text{CO}_2,\text{in}} - \dot{n}_{\text{CO}_2,\text{out}}) + 1/2 \cdot (\dot{n}_{\text{H}_2\text{O},\text{in}} - \dot{n}_{\text{H}_2\text{O},\text{out}})} \quad [\text{Eq. (8)}]$$

$$S_{\text{O},\text{H}_2\text{O}_2} = \frac{\dot{n}_{\text{H}_2\text{O}_2,\text{out}}}{(\dot{n}_{\text{CO}_2,\text{in}} - \dot{n}_{\text{CO}_2,\text{out}}) + 1/2 \cdot (\dot{n}_{\text{H}_2\text{O},\text{in}} - \dot{n}_{\text{H}_2\text{O},\text{out}})} \quad [\text{Eq. (9)}]$$

H-based selectivity:

$$S_{\text{H},\text{H}_2} = \frac{\dot{n}_{\text{H}_2,\text{out}}}{(\dot{n}_{\text{H}_2\text{O},\text{in}} - \dot{n}_{\text{H}_2\text{O},\text{out}})} \quad [\text{Eq. (10)}]$$

$$S_{\text{H},\text{H}_2\text{O}_2} = \frac{\dot{n}_{\text{H}_2\text{O}_2,\text{out}}}{(\dot{n}_{\text{H}_2\text{O},\text{in}} - \dot{n}_{\text{H}_2\text{O},\text{out}})} \quad [\text{Eq. (11)}]$$

Computational Part

0D Chemical Kinetics Model

The plasma chemistry set developed in this work is applied to a zero-dimensional (0D) kinetic model, called Global_kin, developed by Kushner and coworkers,^[84,85] to describe the underlying reactions taking place. The time-evolution of the species densities is calculated, based on production and loss processes, as defined by the chemical reactions. The rate coefficients of the heavy particle reactions depend on the gas temperature and are calculated by Arrhenius equations. The rate coefficients for the electron impact reactions are a function of the electron temperature, and are calculated in the Boltzmann equation module. Finally, the electron temperature is calculated with an energy balance equation. More details about this model can be found in the work of Kushner et al.^[84,85] and in the ESI.

Plasma Chemistry Included In The Model

The data to compile the necessary plasma chemistry, was taken from different sources and expanded with additional $\text{CO}_2/\text{H}_2\text{O}$ interactions. For example, the CO_2 chemistry and the $\text{H}_2\text{O}/\text{O}_2$ chemistry used in this study are mainly adopted from Aerts et al.^[86] and van Gaens et al.^[87] respectively. While the hydrocarbon chemistry, necessary to describe the reactions between CO_2 and H_2O species, and thus for the product formation, was partially taken from Snoeckx et al.^[62] The total chemistry set considers 75 different species (listed in Table 3), which react with each other in 187 electron impact reactions, 346 ion reactions and 369 neutral reactions. Their corresponding rate coefficients and the references where these data were adopted from are listed in ^[62,86,87] and can be found in the SI.

From Table 2 it is evident that several high-value oxygenates, like oxalic acid, formic acid, DME or ethanol, are not included in our model, because of lack of complete data on the specific reaction rate coefficients in literature, needed to describe their formation and loss processes. Of course, we could have incorporated these species, but due to the scarcity of coherent input data, their densities would be subject to such large uncertainties that the predictive character of the model would have less to no value. Furthermore, these oxygenates were not detected in our experiments. In literature, some of them were detected, but this was in a microwave plasma setup, which operates at significantly different conditions than the DBD plasma under study here. Last but not least, as will be illustrated in the chemical analysis section, the oxygenates that are included in the model, such as methanol and formaldehyde, are barely formed (not in the calculations, nor in the experiments), and as the other high value oxygenates (not included in the model) are likely to be formed from the same precursors, one can expect their formation to be of minor importance at the plasma conditions under study, as also supported by their experimental absence. Nevertheless, we hope that rate coefficients for these molecules will become available in literature in the near future, which would allow us to build an even more complete model, and more importantly, to investigate under which other circumstances these oxygenates might be formed.

Additionally, one could wonder whether it is necessary to keep pursuing hundreds of reactions—with their specific coefficients and so on—to perfect chemical kinetics chemistry models. In section ‘Underlying mechanisms for the observed trends’, it was possible to identify 23 different reactions with which a reaction scheme could be compiled and the observed trends explained. This is of course a big difference compared to the 902 different reactions that are included in the model. As such one could indeed wonder about the necessity of including all these reactions. However, it is important to realize this information is evidently only available after the facts, and during the construction of these chemistry sets, missing one (seemingly unimportant) reaction can lead to dramatically wrong outcomes. Therefore, it is absolutely necessary to first build a comprehensive set. Furthermore, building a more complete chemistry set allows this set to be used to model different reactor types and conditions, as was done in this work for the extended range of H_2O concentrations and energy inputs. However, when a relatively complete chemistry model is available in literature (as developed in this work) and one wants to optimize a specific set up, and/or start modeling in two or three dimensions (to include geometry variations for example), from that point on it has no use to continue pursuing an as complete model as possible and one should focus on simplifying the chemistry to its bare essence. The latter is necessary, not only to make the interpretation of the results easier to grasp, but also due to computational restraints, because it is impossible to model a reactor in 3D with hundreds of reactions.

Table 3. Species included in the model

C-O compounds	CO ₂ , CO, C ₂ O, CO ₂ ⁺ , CO ⁺ , CO ₄ ⁺ , CO ₄ ⁻ , CO ₃ ⁻ , C ₂ O ₄ ⁺ , C ₂ O ₃ ⁺ , C ₂ O ₂ ⁺
C compounds	C, C ₂ , C ₂ ⁺ , C ⁺
O compounds	O ₃ , O ₂ , O, O ₄ ⁻ , O ₃ ⁻ , O ₂ ⁻ , O ⁻ , O ₄ ⁺ , O ₂ ⁺ , O ⁺
C-H compounds	CH ₄ , CH ₃ , CH ₂ , CH, CH ₅ ⁺ , CH ₄ ⁺ , CH ₃ ⁺ , CH ₂ ⁺ , CH ⁺
C ₂ -H compounds	C ₂ H ₆ , C ₂ H ₅ , C ₂ H ₄ , C ₂ H ₃ , C ₂ H ₂ , C ₂ H, C ₂ H ₆ ⁺ , C ₂ H ₅ ⁺ , C ₂ H ₄ ⁺ , C ₂ H ₃ ⁺ , C ₂ H ₂ ⁺
C ₃ -H and C ₄ -H compounds	C ₃ H ₈ , C ₃ H ₇ , C ₃ H ₆ , C ₄ H ₂
H compounds	H ₂ , H, H ₃ ⁺ , H ₂ ⁺ , H ⁺ , H ⁻
H-O compounds	H ₂ O, OH, HO ₂ , H ₂ O ₂ , OH ⁻ , H ₃ O ⁺ , H ₂ O ⁺ , OH ⁺
C-H-O compounds	CHO, CH ₂ O, CH ₃ O, CH ₂ OH, CH ₃ OH, CHCO, CH ₂ CO, CH ₃ CO, CH ₂ CHO, CH ₃ CHO, C ₂ H ₅ O ₂
Electrons	e ⁻

Sensitivity Analysis of the Rate Coefficients

Since most of the available reaction rate coefficients in literature are prone to some deviations, we performed a sensitivity analysis for the most important reactions, to give an additional indication of the reliability of the model and the predictive value of the model results, and its uncertainties. Typically, the electron impact reaction rate constants calculated using the two-term Boltzmann equation show an uncertainty of approximately 30 %, while the uncertainty on the rate constants of the most important heavy particle reactions is typically up to 100 %. Therefore, we focused on the most important heavy particle reactions for this sensitivity analysis, more specifically those reactions that play a role in the important reaction paths; see the section on 'Underlying mechanisms for the observed trends'. From this analysis we could conclude that overall, the uncertainties in the rate constants do not cause large deviations in the CO₂ and H₂O conversions, because a variation in the rate constants by 100 % yields only deviations in the calculation results in the order of at maximum 10 %, and typically even lower than 5 %. For more details about this sensitivity analysis we refer to the SI.

Application Of The 0D Model To A DBD Reactor

0D models can only calculate the species densities as a function of time, and thus they neglect spatial variations. Nevertheless, by using the gas flow rate, the time evolution can be translated into a spatial evolution (i.e. as a function of position in the DBD reactor). This spatial evolution is necessary to mimic the typical filamentary behavior found in DBDs used

for CO₂ conversion.^[88] On their way throughout the reactor the gas molecules will pass through several micro-discharge filaments. This is mimicked in the model by applying a large number of consecutive triangular micro-discharge pulses, in the same way as described in our previous work.^[62] This approach has already proven to be applicable for a variety of conditions, gas mixtures and different 0D simulation codes.^[14,33,62,69,73,74,89] The experimental gas flow rate is used, i.e., 600 mL/min at 323 K and atmospheric pressure, with a DBD reactor volume of 15.1 cm³ (see above), thus corresponding to a residence time of 1.66 s.

The model was run at constant temperature of 323 K. In reality, the temperature might change due to the chemical reactions taking place (either exo- or endotherm). Indeed, a considerable fraction of the energy delivered to the plasma will be lost in reaction pathways that eventually lead to the re-formation of the reactants (cf. reactions 1–7), which means that the energy supplied by the electrons to the chemical species will be eventually transformed into other forms of energy (e.g. thermal energy). This energy might lead to a local rise of the temperature, probably limited to the micro-discharge volume, which might affect the chemical reactivity of the system. However, we believe that our assumption of constant temperature is in first instance justified, for the following reasons. (i) There are both exothermic and endothermic reactions in the overall reaction chemistry, and the energy released by the exothermic reactions will be balanced by the endothermic reactions. (ii) In similar work on dry reforming of methane^[42,62] it was demonstrated that the conversion is mainly determined by the (gas temperature independent) electron impact reactions during (and shortly after) the micro-discharge filaments, whereas most of the product formation (and hence the selectivities) are determined by the afterglow reactions. Furthermore, it was observed during temperature-controlled experiments that conversions and selectivity did not change significantly when rising the temperature from 297 K to 473 K.^[42] Nevertheless, to check the validity of the assumption of constant temperature, we have run our model for two additional temperatures, i.e., 373 and 423 K (instead of the standard calculations of 323 K). At 373 K the relative changes in CO₂ conversion compared to the standard calculations are about + 2–4 %, and the relative changes in the H₂O conversion are about + 2 %. At 423 K the relative changes in CO₂ conversion compared to the standard calculations are about + 6–10 %, and the relative changes in the H₂O conversion are about - 10–13 %. The selectivities remained almost unchanged, with only a significant + 20–30 % increase in the O₃ and H₂O₂ concentrations. However, we believe that such heating of the gas temperature in the reactor up to 423 K does not occur, as it was not observed experimentally, mainly due to the small micro-discharge volumes and the cooling due to the continuous gas flow.

Acknowledgements

The authors acknowledge financial support from the Inter-university Attraction Pole (IAP; grant number IAP-VII/12, P7/34) program 'PSI-Physical Chemistry of Plasma-Surface Interactions', financially supported by the Belgian Federal Office for Science Policy (BELSPO), as well as the Fund for Scientific Research Flanders (FWO; grant number G.0066.12N). This work was carried out in part using the Turing HPC infrastructure at the CalcUA core facility of the Universiteit Antwerpen, a division of the Flemish Supercomputer Center VSC, funded by the Hercules Foundation, the Flemish Government (department EWI) and the University of Antwerp. We also would like to thank the financial support given by 'Fonds David et Alice Van Buuren'. Finally, we are very grateful to M. Kushner for providing the Global_kin code,

to T. Dufour for his support during the experiments, and to R. Aerts for his support during the model development.

Keywords: Carbon dioxide • Kinetic modelling • Non-thermal plasma • Plasma chemistry • Water splitting

- [1] R. K. Pachauri, L. A. Meyer, *IPCC, 2014: Climate Change 2014: Synthesis Report. Contribution of Working Groups I, II and III to the Fifth Assessment Report of the Intergovernmental Panel on Climate Change*, Geneva, Switzerland, **2014**.
- [2] J. Albo, M. Alvarez-Guerra, P. Castaño, A. Irabien, *Green Chem.* **2015**, *17*, 2304–2324.
- [3] G. Fiorani, W. Guo, A. W. Kleij, *Green Chem.* **2015**, *17*, 1375–1389.
- [4] W. McDonough, M. Braungart, P. Anastas, J. Zimmerman, *Environ. Sci. Technol.* **2003**, *37*, 434A–441A.
- [5] J. Barber, *Chem. Soc. Rev.* **2009**, *38*, 185–196.
- [6] E. E. Benson, C. P. Kubiak, A. J. Sathrum, J. M. Smieja, *Chem. Soc. Rev.* **2009**, *38*, 89–99.
- [7] M. Aresta, A. Dibenedetto, A. Angelini, *Chem. Rev.* **2014**, *114*, 1709–1742.
- [8] J. R. Scheffe, A. Steinfeld, *Mater. Today* **2014**, *17*, 341–348.
- [9] E. V. Kondratenko, G. Mul, J. Baltrusaitis, G. O. Larrazabal, J. Perez-Ramirez, G. O. Larrazabal, J. Pérez-Ramírez, *Energy Environ. Sci.* **2013**, *6*, 3112–3135.
- [10] A. H. McDaniel, E. C. Miller, D. Arifin, A. Ambrosini, E. N. Coker, R. O’Hayre, W. C. Chueh, J. Tong, *Energy Environ. Sci.* **2013**, *6*, 2424–2428.
- [11] A. Goepfert, M. Czaun, J.-P. Jones, G. K. Surya Prakash, G. A. Olah, *Chem. Soc. Rev.* **2014**, *43*, 7995–8048.
- [12] C. Liu, G. Xu, T. Wang, *Fuel Process. Technol.* **1999**, *58*, 119–134.
- [13] S. Samukawa, M. Hori, S. Rauf, K. Tachibana, P. Bruggeman, G. Kroesen, J. C. Whitehead, A. B. Murphy, A. F. Gutsol, S. Starikovskaia, et al., *J. Phys. D. Appl. Phys.* **2012**, *45*, 253001.
- [14] R. Snoeckx, Y. X. Zeng, X. Tu, A. Bogaerts, *RSC Adv.* **2015**, *5*, 29799–29808.
- [15] G. Chen, T. Silva, V. Georgieva, T. Godfroid, N. Britun, R. Snyders, M. P. Delplancke-Ogletree, *Int. J. Hydrogen Energy* **2015**, *40*, 3789–3796.
- [16] Z. Jiang, T. Xiao, V. L. Kuznetsov, P. P. Edwards, *Philos. Trans. A. Math. Phys. Eng. Sci.* **2010**, *368*, 3343–64.
- [17] M. Mikkelsen, M. Jørgensen, F. C. Krebs, *Energy Environ. Sci.* **2010**, *3*, 43–81.
- [18] G. Centi, E. A. Quadrelli, S. Perathoner, *Energy Environ. Sci.* **2013**, *6*, 1711–1731.
- [19] P. L. Spath, D. C. Dayton, *Natl. Renew. Energy Lab.* **2003**, *December*, 1–160.
- [20] E. Linley, S. P. Denyer, G. McDonnell, C. Simons, J. Y. Maillard, *J. Antimicrob. Chemother.* **2012**, *67*, 1589–1596.
- [21] G. McDonnell, in *New Biocides Dev.*, **2007**, pp. 292–308.
- [22] M. Finnegan, E. Linley, S. P. Denyer, G. McDonnell, C. Simons, J. Y. Maillard, *J. Antimicrob. Chemother.* **2010**, *65*, 2108–2115.
- [23] D. Dobrynin, G. Fridman, G. Friedman, A. Fridman, *New J. Phys.* **2009**, *11*, 115020.
- [24] J. Ehlbeck, U. Schnabel, M. Polak, J. Winter, T. von Woedtke, R. Brandenburg, T. von dem Hagen, K.-D. Weltmann, *J. Phys. D. Appl. Phys.* **2011**, *44*, 13002.
- [25] J. Winter, H. Tresp, M. U. Hammer, S. Iseni, S. Kupsch, a Schmidt-Bleker, K. Wende, M. Dünbier, K. Masur, K.-D. Weltmann, et al., *J. Phys. D. Appl. Phys.* **2014**, *47*, 285401.
- [26] X. Lu, G. V. Naidis, M. Laroussi, S. Reuter, D. B. Graves, K. Ostrikov, *Phys. Rep.* **2016**, *630*, 1–84.
- [27] A. Bogaerts, T. Kozák, K. van Laer, R. Snoeckx, *Faraday Discuss.* **2015**, *183*, 217–232.
- [28] R. Aerts, W. Somers, A. Bogaerts, *ChemSusChem* **2015**, *8*, 702–716.
- [29] S. Heijkers, R. Snoeckx, T. Kozák, T. Silva, T. Godfroid, N. Britun, R. Snyders, A. Bogaerts, *J. Phys. Chem. C* **2015**, *119*, 12815–12828.
- [30] T. Silva, N. Britun, T. Godfroid, R. Snyders, *Plasma Sources Sci. Technol.* **2014**, *23*, 25009.
- [31] A. P. H. Goede, W. A. Bongers, M. F. Graswinckel, R. M. C. M. Van De Sanden, M. Leins, J. Kopecki, A. Schulz, M. Walker, *EPJ Web Conf.* **2014**, *79*, 1005.
- [32] F. Brehmer, S. Welzel, R. M. C. M. Van De Sanden, R. Engeln, *J. Appl. Phys.* **2014**, *116*, 123303.
- [33] T. Kozák, A. Bogaerts, *Plasma Sources Sci. Technol.* **2014**, *23*, 45004.
- [34] L. F. Spencer, A. D. Gallimore, *Plasma Sources Sci. Technol.* **2013**, *22*, 15019.
- [35] A. Indarto, D. R. Yang, J.-W. Choi, H. Lee, H. K. Song, *J. Hazard. Mater.* **2007**, *146*, 309–15.
- [36] T. Nunnally, K. Gutsol, A. Rabinovich, A. Fridman, A. Gutsol, A. Kemoun, *J. Phys. D. Appl. Phys.* **2011**, *44*, 274009.
- [37] X. Tao, M. Bai, X. Li, H. Long, S. Shang, Y. Yin, X. Dai, *Prog. Energy Combust. Sci.* **2011**, *37*, 113–124.
- [38] G. Petitpas, J. Rollier, A. Darmon, J. Gonzalez-Aguilar, R. Metkemeijer, L. Fulcheri, *Int. J. Hydrogen Energy* **2007**, *32*, 2848–2867.
- [39] A. Janeco, N. R. Pinha, V. Guerra, *J. Phys. Chem. C* **2015**, *119*, 109–120.
- [40] G. Scarduelli, G. Guella, D. Ascenzi, P. Tosi, *Plasma Process. Polym.* **2011**, *8*, 25–31.
- [41] Y. Zhang, Y. Li, Y. Wang, C. Liu, B. Eliasson, *Fuel Process. Technol.* **2003**, *83*, 101–109.
- [42] X. Zhang, M. S. Cha, *J. Phys. D. Appl. Phys.* **2013**, *46*, 415205.
- [43] L. M. Martini, G. Dilecce, G. Guella, A. Maranzana, G. Tonachini, P. Tosi, *Chem. Phys. Lett.* **2014**, *593*, 55–60.
- [44] D. Li, X. Li, M. Bai, X. Tao, S. Shang, X. Dai, Y. Yin, *Int. J. Hydrogen Energy* **2009**, *34*, 308–313.
- [45] B. Eliasson, C. Liu, U. Kogelschatz, *Ind. Eng. Chem. Res.* **2000**, *39*, 1221–1227.
- [46] V. J. Rico, J. L. Hueso, J. Cotrino, A. R. González-Elipse, *J. Phys. Chem. A* **2010**, *114*, 4009–4016.
- [47] X. Tu, J. C. Whitehead, *Appl. Catal. B Environ.* **2012**, *125*, 439–448.
- [48] Q. Wang, Y. Cheng, Y. Jin, *Catal. Today* **2009**, *148*, 275–282.
- [49] B. Fidalgo, A. Domínguez, J. Pis, J. Menéndez, *Int. J. Hydrogen Energy* **2008**, *33*, 4337–4344.

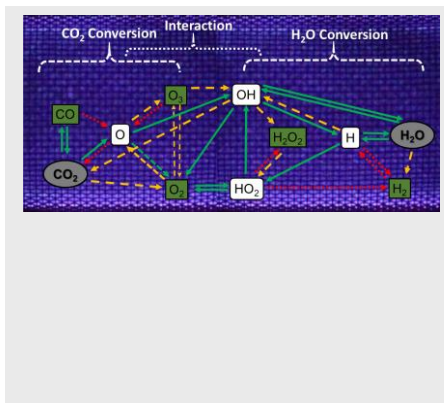
-
- [50] A. Ozkan, T. Dufour, G. Arnoult, P. De Keyzer, A. Bogaerts, F. Reniers, *J. CO₂ Util.* **2015**, *9*, 74–81.
- [51] A. Fridman, *Plasma Chemistry*, Cambridge University Press, New York, **2008**.
- [52] P. Bruggeman, C. Leys, *J. Phys. D: Appl. Phys.* **2009**, *42*, 53001.
- [53] M. A. Malik, A. Ghaffar, S. A. Malik, *Plasma Sources Sci. Technol.* **2001**, *10*, 82–91.
- [54] P. Sunka, V. Babický, M. Clupek, P. Lukes, M. Simek, J. Schmidt, M. Cernák, *Plasma Sources Sci. Technol.* **1999**, *8*, 258–265.
- [55] B. R. Locke, S. M. Thagard, *Plasma Chem. Plasma Process.* **2012**, *32*, 875–917.
- [56] T. Ihara, M. Kiboku, Y. Iriyama, *Bull. Chem. Soc. Jpn.* **1994**, *67*, 312–314.
- [57] T. Ihara, T. Ouro, T. Ochiai, M. Kiboku, Y. Iriyama, *Bull. Chem. Soc. Jpn.* **1996**, *69*, 241–244.
- [58] S. Futamura, H. Kabashima, *Stud. Surf. Sci. Catal.* **2004**, *153*, 119–124.
- [59] S. Mahammadunnisa, E. L. Reddy, D. Ray, C. Subrahmanyam, J. C. Whitehead, *Int. J. Greenh. Gas Control* **2013**, *16*, 361–363.
- [60] N. Hayashi, T. Yamakawa, S. Baba, *Vacuum* **2006**, *80*, 1299–1304.
- [61] L. Guo, X. Ma, Y. Xia, X. Xiang, X. Wu, *Fuel* **2015**, *158*, 843–847.
- [62] R. Snoeckx, R. Aerts, X. Tu, A. Bogaerts, *J. Phys. Chem. C* **2013**, *117*, 4957–4970.
- [63] E. C. Neyts, K. Ostrikov, M. K. Sunkara, A. Bogaerts, *Chem. Rev.* **2015**, *115*, 13408–13446.
- [64] W. Bongers, H. Bouwmeester, B. Wolf, F. Peeters, S. Welzel, D. van den Bekerom, N. den Harder, A. Goede, M. Graswinckel, P. W. Groen, et al., *Plasma Process. Polym.* **2016**, DOI 10.1002/ppap.201600126.
- [65] L. Koen Van, B. Annemie, *Plasma Sources Sci. Technol.* **2016**, *25*, 15002.
- [66] Q. Yu, M. Kong, T. Liu, J. Fei, X. Zheng, *Plasma Chem. Plasma Process.* **2012**, *32*, 153–163.
- [67] D. Mei, X. Zhu, Y.-L. He, J. D. Yan, X. Tu, *Plasma Sources Sci. Technol.* **2015**, *24*, 15011–15021.
- [68] K. Van Laer, A. Bogaerts, *Energy Technol.* **2015**, *3*, 1038–1044.
- [69] R. Snoeckx, S. Heijckers, K. Van Wesenbeeck, S. Lenaerts, A. Bogaerts, *Energy Environ. Sci.* **2016**, *9*, 999–1011.
- [70] N. R. Pinhão, a. Janeco, J. B. Branco, *Plasma Chem. Plasma Process.* **2011**, *31*, 427–439.
- [71] M. Ramakers, I. Michielsens, R. Aerts, V. Meynen, A. Bogaerts, *Plasma Process. Polym.* **2015**, *12*, 755–763.
- [72] B. Eliasson, U. Kogelschatz, B. Xue, L.-M. Zhou, *Ind. Eng. Chem. Res.* **1998**, *37*, 3350–3357.
- [73] R. Snoeckx, M. Setareh, R. Aerts, P. Simon, A. Maghari, A. Bogaerts, *Int. J. Hydrogen Energy* **2013**, *38*, 16098–16120.
- [74] R. Aerts, R. Snoeckx, A. Bogaerts, *Plasma Process. Polym.* **2014**, *11*, 985–992.
- [75] E. C. Neyts, K. Ostrikov, *Catal. Today* **2015**, *256*, 23–28.
- [76] E. Jwa, S. B. Lee, H. W. Lee, Y. S. Mok, *Fuel Process. Technol.* **2013**, *108*, 89–93.
- [77] G. Centi, S. Perathoner, *Catal. Today* **2009**, *148*, 191–205.
- [78] F. Studt, I. Sharafutdinov, F. Abild-Pedersen, C. F. Elkjær, J. S. Hummelshøj, S. Dahl, I. Chorkendorff, J. K. Nørskov, *Nat. Chem.* **2014**, *6*, 320–324.
- [79] S. G. Jadhav, P. D. Vaidya, B. M. Bhanage, J. B. Joshi, *Chem. Eng. Res. Des.* **2014**, *92*, 2557–2567.
- [80] M. Scapinello, L. M. Martini, P. Tosi, *Plasma Process. Polym.* **2014**, *11*, 624–628.
- [81] T. Nunnally, K. Gutsol, a Rabinovich, a Fridman, a Gutsol, a Kemoun, *J. Phys. D: Appl. Phys.* **2011**, *44*, 274009.
- [82] S. Paulussen, B. Verheyde, X. Tu, C. De Bie, T. Martens, D. Petrovic, A. Bogaerts, B. Sels, *Plasma Sources Sci. Technol.* **2010**, *19*, 34015.
- [83] A. Bogaerts, W. Wang, A. Berthelot, V. Guerra, *Plasma Sour. Sci. Technol.* **2016**, *25*, 55016.
- [84] R. Dorai, M. J. Kushner, *J. Phys. D: Appl. Phys.* **2003**, *36*, 1075–1083.
- [85] D. S. Stafford, M. J. Kushner, *J. Appl. Phys.* **2004**, *96*, 2451–2465.
- [86] R. Aerts, T. Martens, A. Bogaerts, *J. Phys. Chem. C* **2012**, *116*, 23257–23273.
- [87] W. Van Gaens, A. Bogaerts, *J. Phys. D: Appl. Phys.* **2013**, *46*, 275201.
- [88] A. Ozkan, T. Dufour, T. Silva, N. Britun, R. Snyders, A. Bogaerts, F. Reniers, *Plasma Sources Sci. Technol.* **2016**, *25*, 25013.
- [89] R. Aerts, X. Tu, W. Van Gaens, J. C. Whitehead, a Bogaerts, *Environ. Sci. Technol.* **2013**, *47*, 6478–85.
-

Entry for the Table of Contents (Please choose one layout)

Layout 1:

FULL PAPER

Artificial photosynthesis—the conversion of CO_2 and H_2O into value-added products—has gained significant interest over the years. Plasmas are intensely investigated for CO_2 conversion, however, few studies exist for the combination of CO_2 and H_2O , and without a good understanding of the underlying mechanisms. This work presents an extensive study elucidating the plasma chemistry by a combination of experiments and computations to provide the necessary insights.



Ramses Snoeckx,* Alp Ozkan,
Francois Reniers and Annemie
Bogaerts

Page No. – Page No.
**The Quest For Value-Added
Products From CO_2 And H_2O In A
Dielectric Barrier Discharge: A
Chemical Kinetics Story**

[a] Title(s), Initial(s), Surname(s) of Author(s) including Author(s): MSc Ramses Snoeckx, Prof. dr. Annemie Department: Department of Chemistry, research gro Institution: University of Antwerp
Title(s), Initial(s), Surname(s) of Author(s) including Author(s): MSc Ramses Snoeckx, Prof. dr. Annemie Department: Department of Chemistry, research gro Institution: University of Antwerp